Corrosion Resistance of a New AL 6013-20 SiC(P) in Salt Spray Chamber

Zaki Ahmad and B. J. Abdul Aleem

(Submitted 22 October 1999; in revised form 7 January 2000)

Aluminum 6013 alloy (0.82Si, 0.95Mg, and 0.35Mn) is finding increasing usage in new aircraft designs, automotives, and structural applications due to its good stretch forming character in T4 temper (solution heat treated and naturally aged to a substantially stable conditions) compared to alloy 2024 (4.4Cu, 0.6Mn, 1.5Mg, and balance Al) and Al 6061 (Si0.51 to 0.71, Fe0.35, Cu0.15, Mn0.85, Mg0.15, 0.25Cr, 0.15Zn, and balanced Al).

The newly developed A1 6013 reinforced with 20 vol.% SiC(P) has a higher strength than its unreinforced counterpart. Whereas the corrosion behavior of A1 6013 has been reported in literature, there is no previous data on A1 6013 reinforced with SiC(P). A knowledge of the corrosion behavior of this alloy is crucial to its applications in aerospace, structural, and automotive industry. The first results of corrosion study of this alloy in 3.5 wt.% Na Cl in a salt spray chamber are presented.

Three tempers F (as fabricated), O (annealed), and T4 (age hardened and stabilized at room temperature) of the alloy A1 6013-30 SiC(P) were exposed to environmental chamber in accordance with ASTM recommended practice. The corrosion rate of the alloy showed a decrease with increased exposure period and after 800 h of exposure no appreciable change in the rate of corrosion was observed. The lowest rate of corrosion (4.83 mdd) was shown by temper T4 followed by tempers F and O after 1200 h of exposure in the increasing order of corrosion rate. Fluctuations in the corrosion rate with time are related to the kinetics of growth and dissolution of $Al(OH)_3$ film, which was detected by fourier transformation infrared (FTIR) spectroscopy (FTIS). The film was composed of an inner compact layer and outer bulk layer dependent on the refreshment rate from the bulk solution. Micrograph examination by scanning electron microscopy (SEM) showed the presence of pits covered by aluminum hydroxide gel, which isolates the pit from the bulk solution. The acidic conditions of pits also cause intergranular attack. Pitting was observed to be less pronounced in temper T4 compared to F and O tempers, the former also showing the highest resistance to corrosion.

The data generated predict promising application potential of this alloy in environment where resistance to corrosion is also a major consideration.

Keywords	corrosion, aluminum alloy 6013-20 SiC(P), metal matrix composites, NaCl salt spray test

1. Introduction

During the 1970s, intense desalination activity in the Arabian Gulf region was a driving force behind the search for strong, corrosion-resistant, and economically compatible materials for desalination and process industries. Aluminum alloys 5052 and 6061 have been extensively investigated because of their good corrosion resistance in marine environment and attractive application potential in chemical, petrochemical, and power utilities.[1,2,3] A number of studies on the localized corrosion of aluminum alloys of 5000 and 6000 series have been made.[4,5,6] These alloys were the focus of intensive research because of their low production cost, low maintenance cost, and their nontoxicity in sea coastal environment. Their suitability was amply demonstrated under thermal desalinating conditions.[7,8,9] Cupro-nickel alloys are the best material available; however, because of their high cost and problems arising out of velocity and water chemistry, research and development efforts have been diverted to produce aluminum alloys that could be substituted for conventional and more accepted aluminum alloys.[10–13] The situation has, however, changed in the last decade and attention is shifting gradually from the conventional materials to high performance polymers, advance ceramics, and composites for applications ranging from process to defense industry. Aluminum alloy 6013 has been the focus of attention in recent years because of its improved mechanical properties over the better known alloy A1 6061 and its promising application in aerospace, automobile, and power generation industries. Al 6013 reinforced with 20 vol.% silicon carbide, in particulate form, was designed to have improved mechanical properties, over those or Al 6061 SiC(P), and a better corrosion resistance than Al 2124 SiC(P) T4. Whereas the development of alloy 6013 reinforced with SiC has generated substantial interest, published corrosion data on it is virtually nonexistant. The corrosion resistance of this alloy in marine environment has been recently reported by the authors.[14,15] This paper reports the corrosion resistance of Al 6013-20 SiC(P) T4 in salt spray chamber, which is considered to be a useful tool to evaluate the corrosion resistance of materials in simulated marine environment.

Zaki Ahmad and **B. J. Abdul Aleem,** Mechanical Engineering Department, King Fahd University of Petroleum & Minerals, Dhahran 31261, Saudi Arabia.

2. Experimental

A Singleton salt spray (fog) testing cabinet was used to investigate the corrosion resistance of Al 6013-20 SiC(P). It is comprised of a basic chamber, level-matic reservoir (10 gal.), salt solution reservoir (30 gal.), bubble tank, twin optifog

assembly, and atomizers, as shown in Fig. 1 and 2. Accessories, such as tower assembly, bubble tank heater, level-matic control valve, salt solution valves, level-matic solution valves, and cabinet heaters are the pertinent parts of the equipment.

The level-matic reservoir (10 gal.) and bubble (saturation) tank are filled with demineralized water. The cover water trough located at the top rim of the cabinet is filled with demineralized water (1 in. deep). A salt solution is prepared by adding 8 oz. of sodium chloride per gallon of distilled water. The solution is filtered through a 5 μm polypropylene felt. The solution is transferred to the salt solution reservoir located below the level-matric reservoir. The brass valve on the bottom of the unit is opened to allow the solution by gravity into the optifag lower reservoir located inside the cabinet. A constant level salt solution is maintained. The bulk solution preparation and filtration of the solution is facilitated by the optimum salt solution mixing and storage tank. The brass valve located at the base of the bubble tank is opened to allow the air flow through the tower. Salt spray (fog) is introduced into the cabinet from the optifog assembly in which a constant level of salt solution is maintained. The bubble tank internal air pressure is maintained between 12 and 18 psi. The thermologic digital temperature controller maintains the cabinet interior bubble level at 15 psi. The pH of the solution when atomized is maintained at 7.4 by adjusting with HCl. The compressed air supply was maintained at 130 kN/m^2. All experiments were conducted at 35 °C (±1 °C).

Rectangular specimens of A1 6013-20 SiC(P) in O, F, and T4 tempers were used. The samples were polished with 320, 400, and 600 grit SiC and finally polished with a 6 and 1 μm diamond paste in nap cloth for 1 and 1.5 min, respectively, followed by rinse in demineralized water and ethyl alcohol. After exposure for 200 h, the samples were gently washed in clean and running water to remove salt deposit.

Separate weight-loss studies were conducted at 100 °C in 3.5wt.%NaCl in recirculating loop under condition of smooth flow. The loop was designed by the authors and describe elsewhere.[16] Circular specimens measuring 2.5 cm and 2 mm thick were used for weight-loss studies. Polished specimens were used for weight-loss studies.

Corrosion rates were calculated from the following relationships.

$$P = \frac{W \times 365 \times 1000}{ATD} \quad \text{(Eq 1)}$$

where

P = average penetration rate, mm/annum;
W= mass loss, g;
A = initial exposed surface, mm^2;
T = exposure period, d; and
D= density of the material g/cm^3.

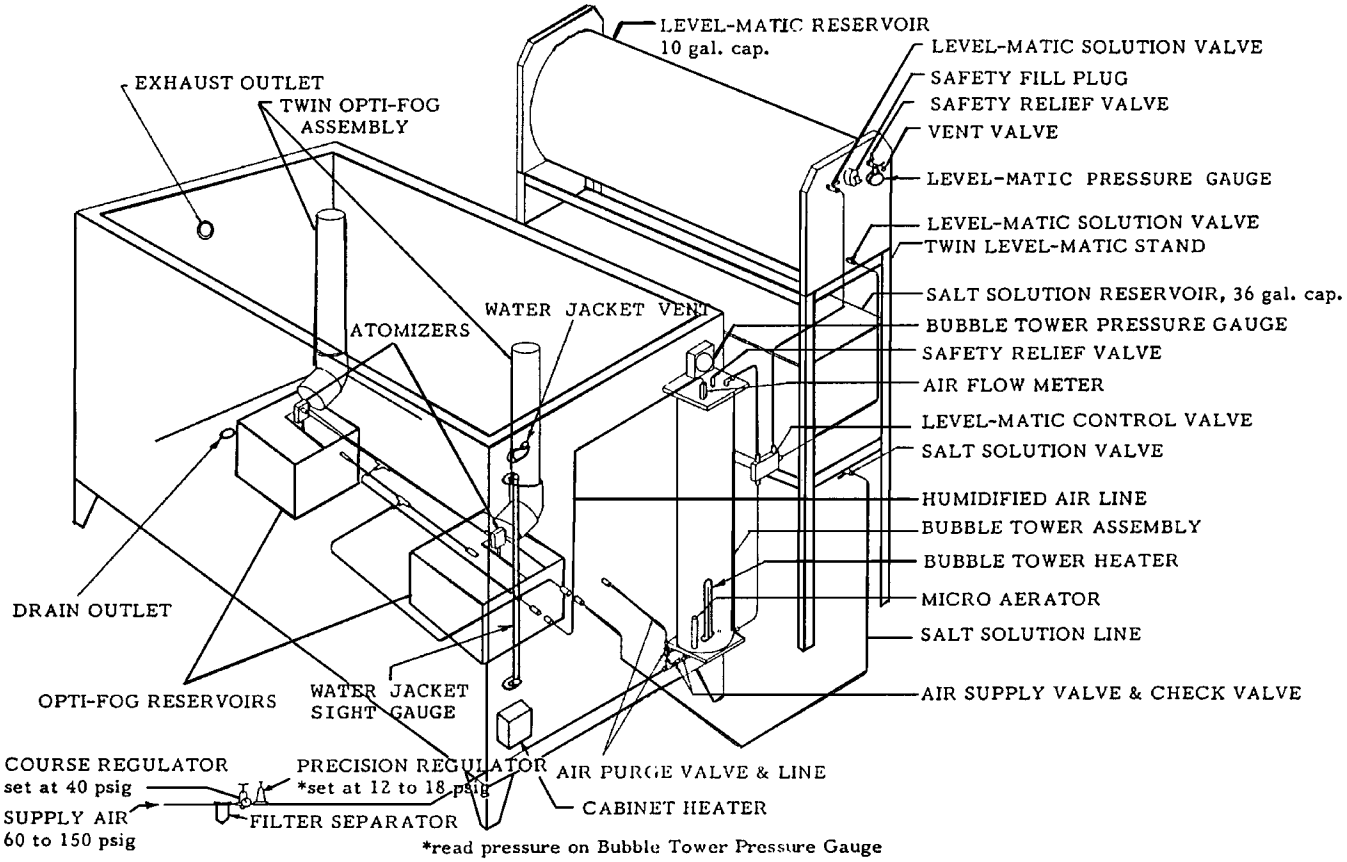

Fig. 1 Singleton salt fog corrosion test cabinet—number 23, 24, or 25

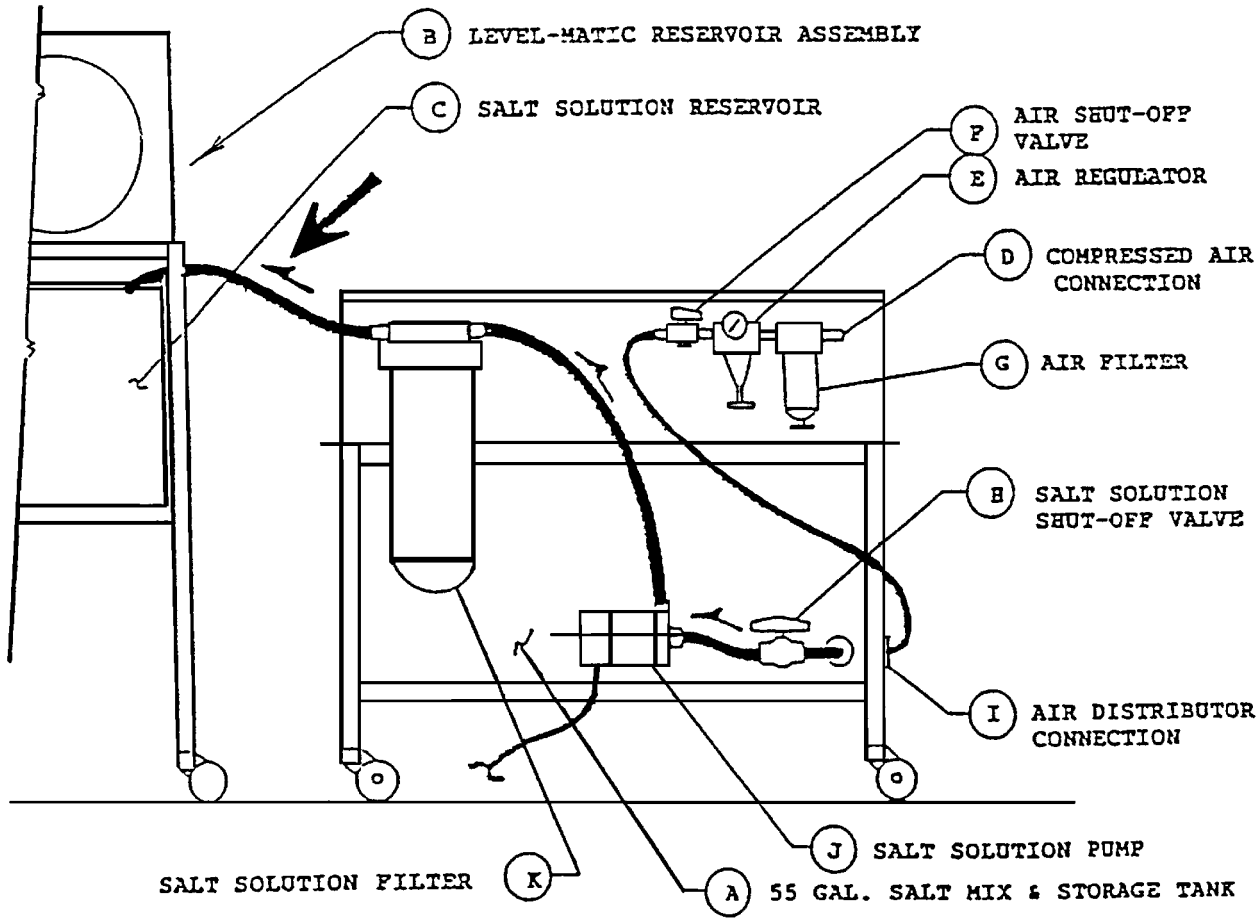

Fig. 2 Cross section of singleton salt fog corrosion test cabinet

$$P = \frac{W \times 365 \times 1000}{ATD(2.54)^3} = \frac{2.27 \times 10^4 W}{ATD} \quad \text{(Eq 2)}$$

where

P = average penetration rate, mpy
W = mass loss, g
A = initial exposed surface area, in2
T = exposure time, d

Metallographic studies were conducted by scanning electron microscopy on corroded and uncorroded samples.

3. Results and Discussion

The variation of corrosion rate of three tempers of O, F, and T4 of alloy 6013–20 SiC(P) in salt spray chamber is shown in Table 1. The highest corrosion rate was shown by temper O (10.23 mpy), followed by temper F (8.42 mpy) and temper T4 (7.12 mpy) in decreasing order after 200 h. The corrosion rate, however, showed a continuous decline with increased exposure exemplified by a decrease in the corrosion rate from 10.23 to 4.27 mpy, 8.42 to 3.68 mpy, and 7.12 to 4.27 mpy after 1200 h of exposure to salt spray environment. The phenomena of decreased corrosion rate with increased exposure period have also been observed in other aluminum alloys, such as Al alloys 6063 and 5052,[17] and it is ascribed to the kinetics of film formation and film dissolution and change in the composition of the film from being beyrite to boehemite.[18,19] The observed decrease in the rate of corrosion is consistent with the time dependence of anodic reaction, the cathodic reaction being independent of time. Studies on A1 alloys of 6000 and 5000 series have adequately shown that the film formation by corrosion product has a beneficial effect on the corrosion rate.

Separate weight-loss studies at elevated temperatures were conducted in 3.5 wt. % NaCl for 100 and 200 h. The results of the studies are shown in Tables 2 and 3. A three- to fourfold increase in the rate of corrosion was observed on increasing the temperature from 50 to 75 °C, whereas a much lesser increase was observed between 75 and 100 °C. The above observation confirms the belief that the corrosion behavior of A1 6013-20 SiC is a very strong function of $Al(OH)_3$, and once the film formation is complete, it becomes independent of oxygen.[20] The relative decrease in the rate of corrosion observed on increasing the temperature from 50 to 75 °C is attributable to a change in the composition of the film from boehemite Al_2O_3, $3H_2O$ to Al_2O_3, H_2O (boehemite to beyrite), which has been identified by Fourier transformation infrared (FTIR) spectroscopy studies.

Table 1 Variation of corrosion rate of Al-6013-20 SiC(P) by salt spray (fog) testing

	Corrosion rates					
	O-temper		F-temper		T4-temper	
Time (h)	mpy	mdd	mpy	mdd	mpy	mdd
200	10.23	19.18	8.42	15.78	7.12	13.35
400	9.11	17.08	7.78	14.58	6.18	11.59
600	6.38	11.96	5.06	9.49	4.38	8.21
800	4.92	9.23	3.98	7.46	2.82	5.28
1000	4.66	8.74	3.76	7.05	2.63	4.93
1200	4.27	8.01	3.68	6.90	2.58	4.83

To convert mpy to mm/yr, multiply by $10^{-3} \times 25.4$
To convert mdd to mm/yr, multiply by $0.03652/\rho$ (ρ density in g/cm^3)

Table 2 Variation of corrosion rate of Al-6013-20 SiC(P) with temperature in 3.5% NaCl (static condition for 100 h exposure time)

	Corrosion rate (open air condition)						Corrosion rate (deaerated condition)					
	O-temper		F-temper		T-4-temper		O-temper		F-temper		T-4-temper	
Temperature (C°)	mpy	mdd	mpy	mdd	mpy	mdd	mpy	mdd	mpy	mdd	mpy	mdd
50	1.90	3.56	1.09	2.04	0.43	0.80	1.51	2.83	0.97	1.81	0.34	0.637
75	5.96	11.17	5.16	9.67	4.6	8.62	4.76	8.92	4.28	8.02	3.97	7.44
100	7.46	13.98	6.96	13.05	5.8	10.87	6.7	12.56	6.3	11.81	4.50	8.43

To convert mpy to mm/yr, multiply by $10^{-3} \times 25.4$
To convert mdd to mm/yr, multiply by $0.03652/\rho$ (ρ density in g/cm^3)

Table 3 Variation of corrosion rate of Al-6013-20 SiC(P) with temperature in 3.5%NaCl (static condition for 200 h exposure time)

	Corrosion rate (open air condition)						Corrosion rate (deaerated condition)					
	O-temper		F-temper		T-4-temper		O-temper		F-temper		T-4-temper	
Temperature (C°)	mpy	mdd	mpy	mdd	mpy	mdd	mpy	mdd	mpy	mdd	mpy	mdd
50	2.14	4.01	1.72	3.22	1.11	2.08	1.27	2.38	1.37	2.56	0.98	1.83
75	6.74	12.63	5.83	10.93	5.98	11.21	5.16	9.67	5.11	9.58	4.87	9.13
100	8.2	15.37	7.3	13.68	6.20	11.62	7.10	13.31	6.63	12.43	4.96	9.30

To convert mpy to mm/yr, multiply by $10^{-3} \times 25.4$
To convert mdd to mm/yr, multiply by $0.03652/\rho$ (ρ density in g/cm^3)

The decrease in the rate of corrosion in 3.5wt.%NaCl compared to salt spray test is the result of a highly aggressive environment in the latter.

Examination of corroded surfaces revealed pitting and intergranular corrosion as the predominant form of localized corrosion. The type of pits ranged from being shallow and crystallographic to deep. Some salt particles were observed on the alloy surface. The surface of the alloy is often covered with a white gelatinous product of aluminum hydroxide $Al(OH)_3$. The pit environment is highly acidic. The hydroxide gel formed isolates the pit from the bulk solution. As bubbles of hydrogen rise from the surface, corrosion chimneys are formed. The hydrogen bubbles pump up $AlCl_x$ $(OH)_{3-n}$ to the outside, which reacts with water to form $Al(OH)_3$.[21] Figure 3 shows corrosion products with corrosion chimneys. Figure 4 shows a typical pit corrosion chimney and silica particle in O temper of the alloy exposed to salt spray test. Crystallographic faceting in O temper can be observed in Fig. 5. The surface morphology of F temper of the alloy shows a variety of features. SiC particles are shown by ABC and the pit D in Fig. 6. The average pit depth observed in F temper was 47.33 m compared to O temper(68.00 μm). The pit depths were of a lower magnitude in T4 temper compared to F and O tempers. The scanning electron microscopy (SEM) photomicrograph of Al 6013-20 SiC(P) T4 is shown in Fig. 7. Preferential dissolution is observed in A. A highly faceted structure indicative of a lesser metal dissolution is shown in Fig. 8. Corrosion chimneys are also shown. Shallow crystallographic pits in a highly ordered pattern are shown in Fig. 9. It has been shown by

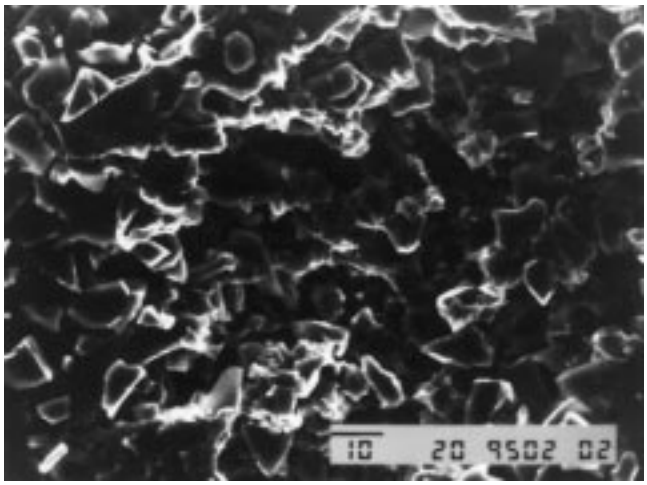

Fig. 3 SEM photomicrograph of Al 6013-20 SiC(P)-OT sample exposed to salt spray test showing corrosion chimneys

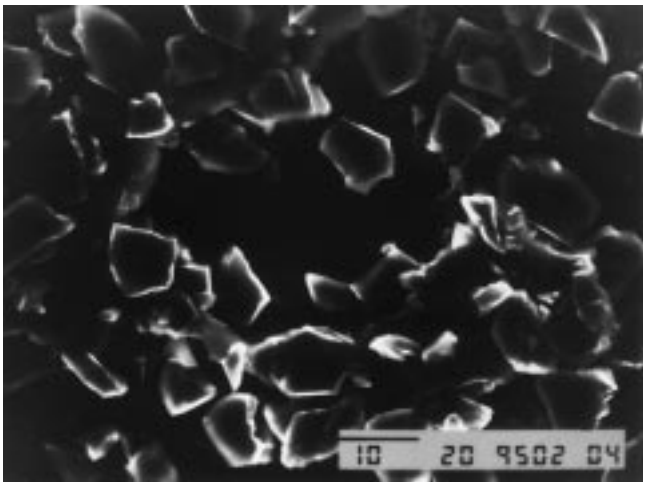

Fig. 5 SEM photomicrograph of Al 6013-20 SiC(P)-OT sample exposed to salt spray, showing crystallographic faceting

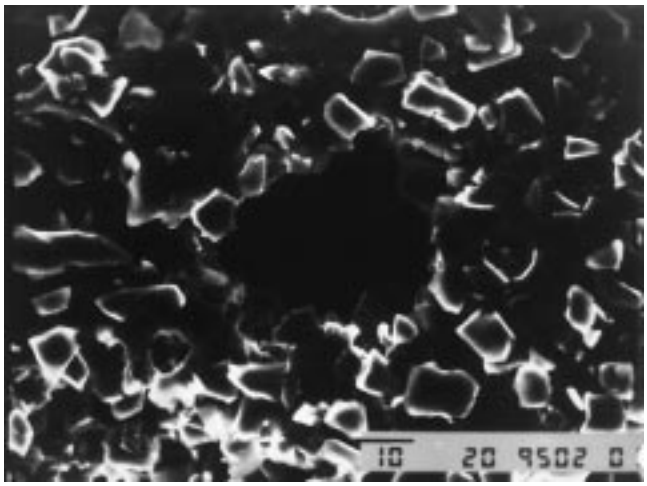

Fig. 4 SEM photomicrograph of Al 6013-20 SiC(P)-OT sample exposed to salt spray test showing pit, corrosion chimney, and silica particle

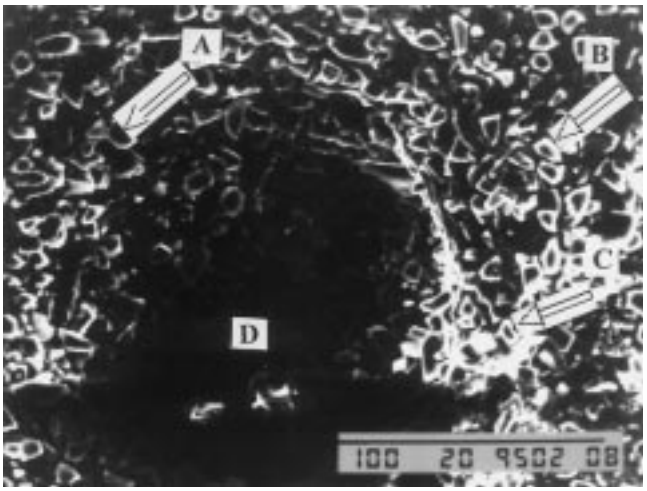

Fig. 6 SEM photomicrograph of Al 6013-20 SiC(P)-F sample exposed to salt spray test. Silica carbide particles are shown by A, B, C and pit is shown by D

micrographic examination that pitting is less pronounced in temper T4 compared to O and F tempers.

Unlike conventional aluminum alloys, the corrosion mechanism of Al-SiC composites is presently not known. For instance, the sites of nucleation of pits, whether they initiate on SiC/Al matrix interface, or on secondary phase particle, or on sites of microsegregation of secondary phases, have not been established. It is, however, believed that the distribution of SiC particles (uniform or agglomeration) and particle of secondary phase, such as Fe, Mn, and Cu, influences the uniformity and thickness of $Al(OH)_3$ film, which has a predominant influence on the corrosion kinetics. Whether the film would develop weak spots or it would be uniform would depend on the concentration of secondary phase particles, cathodic precipitates, SiC particles, and distribution of SiC particles. Sufficient evidence has been gathered by the authors to show that a high concentration of intermetallic at Al/SiC interphase is the preferred site for localized corrosion.

4. Conclusions

On the basis of the investigations conducted, the following are the conclusions.

- The corrosion rate of three tempers O, F, and T4 of the alloys in salt spray chamber decreases on increasing the exposure period from 200 to 1200 h. The least rate of corrosion rate of 2.58 mpy (4.8 mm/yr) is exhibited by temper T4 followed by temper F (3.68 mpy) 6.90 mdd, and temper O (4.27 mpy) 8.01 mdd in decreasing rate order of corrosion resistance. A similar trend is shown by the three tempers in weight-loss tests conducted in 3.5wt.%NaCl in a recirculating loop at 50 and 100 °C. The overall rate of corrosion shown by alloy 6013-20 SiC(P) in weight-loss tests was observed to be lower than observed in the salt spray tests.

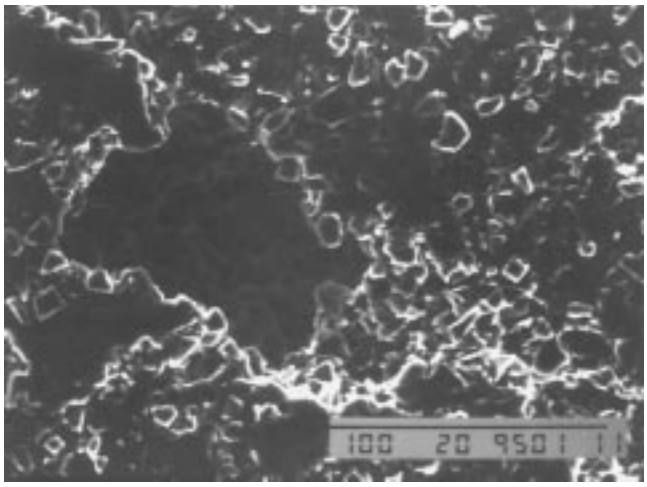

Fig. 7 SEM photomicrograph of Al 6013-20 SiC(P)-T4 sample exposed to salt spray test, showing preferential dissolution

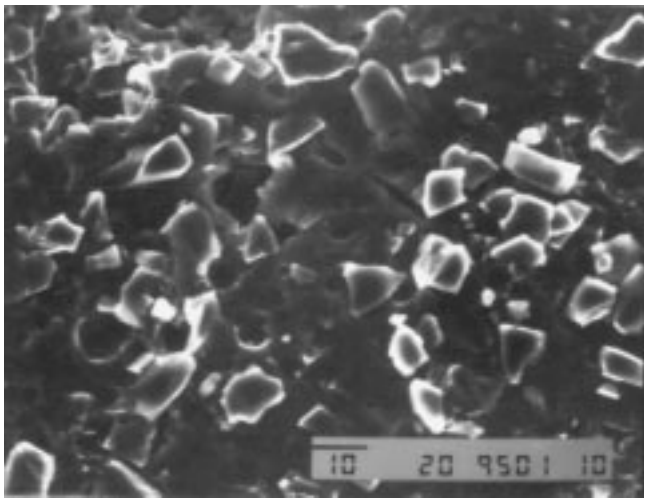

Fig. 8 SEM photomicrograph of Al 6013-20 SiC(P)-T4 sample exposed to salt spray test, showing highly faceted structure with shallow pits

- The rate of corrosion of the three tempers of A1 6013-20 SiC decreased on increasing the temperature from 50 to 100 °C. This phenomenon has been attributed to the changes in the composition of the film from being beyrite (Al_2O_3, H_2O) to boehemite ($-Al_2O_3$, H_2O), as shown by FTIR studies.
- Pitting is the major form of localize corrosion, and corrosion chimneys are formed because of the formation of aluminum hydroxide.

Acknowledgment

The authors acknowledge the financial support provided by KACST and the encouragement and facilities provided by KFUPM.

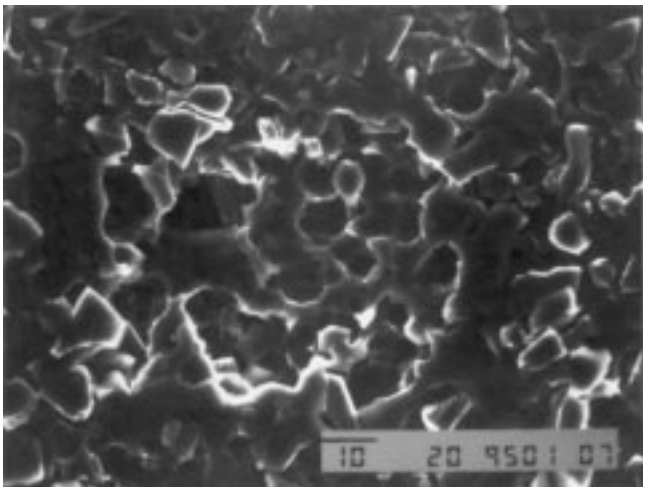

Fig. 9 SEM photomicrograph of Al 6013-20 SiC(P)-T4 sample exposed to salt spray test, showing shallow crystallographic pits in a highly ordered pattern

References

1. W.H. Ailor, Jr.: *Aluminum Alloys after Five Years in Service*, ASTM-STP 445, ASTM, Philadelphia, PA, 1969, pp. 115-30.
2. E.T. Wanderor and M.W. Wei: *Metal Congress*, Chicago, IL, Oct. 1966.
3. R.A. Bonewitz: *Corrosion*, 1973, vol. 29 (6), p. 215.
4. E.D. Vernik, Jr.: *A Progress Report*, Annual Meeting of the National Association of Corrosion Engineers, St. Louis, MO, Mar. 1972.
5. W.W. Binger and H.W. Frittis: *Corrosion*, 1954, p. 425.
6. I.G. Bohlmann and F.A. Posey: *Proc. 1st Int. Symp. on Water Desalination*, 1965, vol. I, p. 306.
7. R.L. Lindberg: *Mater. Performance*, 1972, vol. II, p. 45.
8. J.N. Wanklyn, N.J.M. Wilkins, D.R.V. Silvester, C.E. Austing, and P.F. Lawrence: *Desalination*, 1971, vol. 9, p. 245.
9. M. Elboujdaini, E. Ghali, R.G. Barradas and M. Girgis: *Corr. Sci.*, vol. 30 (8/9), pp. 855-67, 1990.
10. M.S. Parvizi, A. Aladjem, and J.E. Castle: *Int. Mater. Rev.*, 1988, vol. 33 (4).
11. M.S. Parvizi, A. Aladjem, and J.E. Castle: NCRA Project 2541, Guildford, Surrey, Nov. 1985.
12. W.W. Kirk: Final Report PRJ-384, INCRA, Laque Center for Corrosion Technology, Wrightsville Beach, NC.
13. A.L. Greger and J. Andrew Wacks: *JOM*, 1991, vol. A3 (8), p. 815.
14. Z. Ahmad and B. J. Abdul Aleem: *Corrosion*, 1996, vol. 52 (11), p. 857.
15. Z. Ahmad: KACST Report 1, AR-1465, KACST, Riyadh, Saudi Arabia, p. 85.
16. Z. Ahmad: *Br. Corr. J.*, vol. 33, No. 3, 1998, p. 230.
17. R.A. Bonewitz: *Corrosion*, 1979, vol. 30 (2), p. 253.
18. K.M. Carlson: *Int. J. Electrochem. Soc.*, 1957, p. 147.
19. R.A. Bonewitz: *Corrosion*, 1973, vol. 29 (6) p. 215.
20. A.M. Beccaria, G. Paggi, D. Gingaud, and P. Castellor: *Br. Corr. J.*, 1994, vol. 29 (1), p. 65.
21. T.D. Burleigh, E. Ludwiczak, and R.A. Petro: *Corr. Sci.*, 1995, vol. 51 (1), p. 50.